Accepted Manuscript

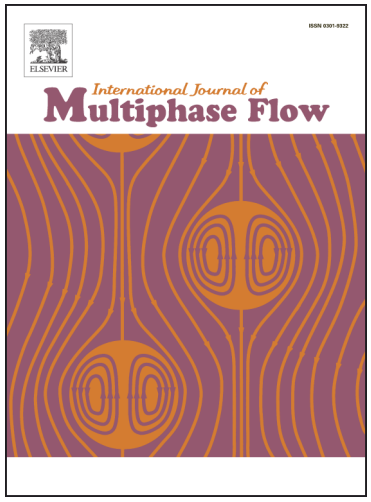

Experimental and numerical study on isolated and non-isolated jet behavior through centrifuge spinning system

Afsaneh Valipouri, Seyed Abdolkarim Hosseini Ravandi, Ahmadreza Pishevar, Emilian I. Părău

PII: S0301-9322(14)00192-X
DOI: http://dx.doi.org/10.1016/j.ijmultiphaseflow.2014.10.005
Reference: IJMF 2110

To appear in: *International Journal of Multiphase Flow*

Received Date: 3 February 2014
Revised Date: 19 June 2014
Accepted Date: 9 October 2014

Please cite this article as: Valipouri, A., Ravandi, S.A.H., Pishevar, A., Părău, E.I., Experimental and numerical study on isolated and non-isolated jet behavior through centrifuge spinning system, *International Journal of Multiphase Flow* (2014), doi: http://dx.doi.org/10.1016/j.ijmultiphaseflow.2014.10.005

Experimental and numerical study on isolated and non-isolated jet behavior through centrifuge spinning system

Afsaneh Valipouri[1], Seyed Abdolkarim Hosseini Ravandi[1*], Ahmadreza Pishevar[2], Emilian I. Părău[3]

[1]*Department of Textile Engineering, Isfahan University of Technology, Isfahan, 84156, Iran*

[2] *Department of Mechanical Engineering, Isfahan University of Technology, Isfahan, Iran*

[3] *School of Mathematics, University of East Anglia, Norwich, NR4 7TJ, United Kingdom*

[*]Corresponding author email: hoseinir@cc.iut.ac.ir

Abstract

This work presents a comparison between an isolated and a non-isolated curved liquid jet emerging from a rotating nozzle through centrifuge spinning system. In the centrifugal spinning process, a polymer solution has been pushed by the centrifugal force through small nozzle of a rapidly rotating cylindrical drum. Thereby thin fibers are formed and collected on a collector in the form of a web. Centrifuge spinning suffered from a strong air resistance which leads to a more deflected jet as well as its rapidly solvent evaporation resulting in thicker nanofibers. In this work, centrifuge spinning has been equipped by a rotating collector, whereas the fabrication process was skillfully sealed from ambient airflow. A comparison was drawn between the trajectory of Newtonian liquid jets fabricated by centrifuge spinning and air-sealed centrifuge spinning. The captured images of the liquid jet trajectory using a high speed camera showed that non-isolated liquid jets were more curved than isolated liquid jets due to air resistance. A pre-presented non-linear analysis of the

Navier-Stokes equations was carried out and the numerical solutions were compared with the experiments.There was fairly good agreement between the isolated jet trajectory and the model-predicted one, but there were differences between the non-isolated jet trajectory and the simulation results. The non-isolated jet curved more compared to the others due to air drag. Also, the diameter of polymeric nanofibers was predicted and compared with experiments. Some qualitative agreement was found.

Keywords

Air-sealed centrifuge spinning, Curved liquid jet, Isolated and non-isolated liquid jet, Air drag, Navier-Stokes equations, Asymptotic expansions.

Introduction

Nanofibers, defined as fibers with diameters of 100 nm to 500 nm [1], are desirable enhancements for a number of promising applications including medical textile [2, 3], filtration [4-6], protective textile [7], electronics [8], and optics[9].

Among the various methods used so far for producing nanofibers, such as drawing [10], template synthesis [11, 12], and self-assembly [13], electrospinning is a well-established and intensively investigated methodology, and is currently the only known technique that can fabricate continuous nanofibres [14-16].

The major challenge associated with electrospinning is its production rate, compared with that of conventional fiber spinning. So far, several efforts have been made to increase the production rate of nanofibers. For instance, modified single-needle [17, 18], multi-needle [19-27], needleless systems [28-34], a plastic filter set-up [35] and forcespinning have been developed to enhance nanofiber production rate. Forcespinning^{TM} or centrifuge spinning uses centrifugal force, rather than electrostatic force, as in the electrospinning process [36]. The

previous researches have indicated that applying the centrifugal force results in a significant increase in the production rate of nanofibers [36, 37]. Due to centrifugal force, the polymer solution sustained by its surface tension is radially transported outward through the nozzle. There is a critical rotational speed of the spinning head for which the centrifugal force finally overcomes the surface tension and the jet of the fluid is ejected from the tip of the nozzle. Centrifugal force, Coriolis force, viscous effects, and air drag are experienced by the jet in centrifuge spinning [38]. The jet follows a curved trajectory due to Coriolis and drag forces. An effect of air resistance is the deflection of the jet and causes the liquid jet to progressively bend up. Another effect of air resistance is the enhancement of surface instabilities [39]. Exposing the ejected liquid jet to the high velocity airflow causes the jet to lose its solvent rapidly and as a consequence, the extension of the jet becomes more difficult, resulting in thicker nanofibers as the other effect of air resistance [40]. It would be interested in eliminating the air resistance included in centrifuge spinning which will be discussed through the present work.

Study on the formation of droplets under rotating forces was done by Wallwork et al. and Decent et al [41, 42]. In their study of the prilling process for producing fertilizers, one-dimensional model equations were derived from the assumption that the flow is uniaxial and the center-line of the jet is steady at the leading order. Furthermore, a linear stability analysis of the derived inviscid model is performed in [41] and for the viscous model in [43].

Other works regarding curved liquid sheets and jets include Vanden-Broeck and Keller [44], Entov and Yarin [45], Dias and Vanden-Broeck [46], Yarin [47] and Cummings and Howell [48]. In particular, Dias and Vanden-Broeck [44] investigated steady two-dimensional inviscid solutions with gravity, determining the trajectory of the flow, and Cummings and Howell [44] investigated nearly straight slender viscous fluid fibers arising in extrusion problems.

E.I. Parau et. al. [49] presented a theoretical investigation of the effects of changing operating parameters on the break-up of curved liquid jets in stagnant air at room temperature and pressure. The Navier–Stokes equations were solved in this system with the usual viscous free-surface boundary conditions, using an asymptotic method based upon a slender-jet assumption without considering the effect of air resistance [49]. However, air resistance has significant effects on liquid jet dynamic. These effects could be incorporated into the theory by including air resistance into the equations of motion. A theory to include air resistance is probably doable, but not very simple. Therefore, neglecting air resistance causes some differences between simulation and experimental results. However, reducing air resistance makes possible to neglect the effects of air resistance on liquid jet dynamic; this would be obtained in the present work. It is expected that there will be an improvement in the agreement between simulations and experimental data.

So far various one-dimensional electrospinning models have been proposed with a focus on the effects of the rheological properties of the polymer solutions on fiber formation [50, 51]. Models describe all the stages of the electrospinning process using both linear and nonlinear models and incorporating the effects of solution viscosity, solvent evaporation and solidification, surface tension, and electric forces [21, 52]. Some of the factors mentined above are included in centrifuge spinning. In addition, rotational speed has significant effect on fiber formation. In current work, the effect of rotational speed on fiber morphology has been theoreticaly and experimentally studied.

Therefore, the first aim of this work is to introduce air-sealed centrifuge spinning for the fabrication of nanofibers. This setup has been isolated from the surrounding air using a rotating collector. In our case, air resistance is negligible because of setup isolation. In addition, a comparison is drawn between trajectory of Newtonian liquid jets as well as non-Newtonian jet fabricated by centrifuge spinning and ones fabricated by air-sealed centrifuge

spinning. Images were captured of the jet trajectory using a high speed camera. Also, a non-linear analysis of the Navier-Stokes equations was carried out. The experimental results were compared to numerical solutions of equations. Further, the diameter of poly acrylonitrile (PAN) nanofibers was predicted and compared with experiments.

Materials and methods

Physical properties of liquids and solutions

The physical properties of three Newtonian fluids are given in Table 1. The trajectory of these fluids was captured during fabrication process.

Table 1. Measured physical properties of Newtonian fluids

Newtonian fluid	Physical properties		
	Viscosity (cp)	Density (g/cm^3)	Surface tension (N/m)
Water	1	1	0.0728
Ethanol	1.2	0.789	0.0223
Acetone	0.36	0.79	0.023

Poly (acrylonitrile) (PAN) with Mn = 70000 g/mol and Mw = 100,000 g/mol was obtained from Iran Polyacryle Co. and used as received. N, N- dimethyl formamide (DMF) from Merck was used as the solvent of PAN. PAN powder was dissolved in DMF into solution with 13 wt% concentration at ambient temperature and was gently stirred for about 24 h to prepare a homogenous solution for spinning. The viscosity and surface tension of PAN solution were measured as 784 cp and 38.44 mN/m, respectively.

Air-sealed centrifuge spinning and Centrifuge spinning

Air-sealed centrifuge spinning setup is schematically shown in Figure 1. Air-sealed centrifuge spinning setup consists of a rotating drive shaft (A), a transparent plate(B), a rotating cylindrical receptacle (C), a metallic cylindrical collector (D), and a movable transparent door (E). The rotating cylindrical receptacle holds a syringe containing polymer solution. The needle attached to the syringe has a 300 µm outer diameter with a wall thickness of 70 µm and a length of 18 mm. Polymer solution is ejected from the needle tip. The distances from the nozzle tip to the rotation center and to the collector are adjusted to 5.3 cm and 8 cm, respectively. The receptacle and the collector are firmly affixed to the drive shaft by the transparent plate. The movable transparent door is used to prevent air from entering and exiting. Hereafter, we call the collection of the receptacle, the nozzle, the collector, the transparent plate, and the movable transparent door, the head of spinning or spinning head.

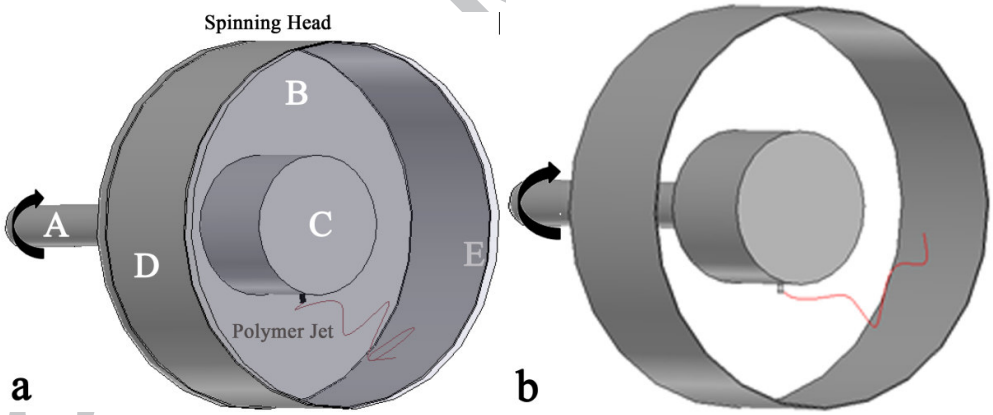

Figure 1. (a) Schematic of air-sealed centrifuge spinning system, (A) rotating drive shaft (B) transparent plate (C) rotating cylindrical receptacle (D) rotating metallic cylindrical collector (E) movable transparent door (b) Schematic of centrifuge spinning system

Centrifuge spinning essentially consists of an axle of rotation, a cylinder to hold syringe, and a metallic cylindrical collector. The collector is stationary and does not contact to other parts of apparatus. Syringe with its holder is rotated by an axel. The difference between centrifuge

spinning and air-sealed centrifuge spinning is that the collector of air-sealed centrifuge spinning is rotated by the axel and the spinning head is sealed from the air. As a result, when air-sealed centrifuge spinning is rotated, the surrounded air through spinning head rotates with the same angular velocity and the air drag force is negligible. While, when centrifuge spinning is rotated, a strong airstream is created around the nozzle. Therefore, it is expected that liquid jet fabricated by centrifuge spinning is more bent up than a liquid jet produced via air-sealed centrifuge spinning. Also, fabrication of thicker nanofibers can be anticipated through centrifuge spinning because of exposing the liquid jet to the high velocity airflow. In fact, high velocity airflow causes the jet to lose its solvent rapidly and as a consequence, the extension of the jet becomes more difficult, resulting in thicker nanofibers, while air-sealed centrifuge spinning has good ability to produce finer nanofibers.

Jet trajectory determination

The trajectory of the liquid jet was captured by means of a high speed digital camera (Canon EOS 400D). The images from the camera were downloaded into a personal computer for analysis. Digital measurements were obtained using image analysis software (Digimizer4).

Fiber diameter characterization

The morphology of nanofiber mats was characterized using a FESEM (Hitachi S-4160) instrument. Before the FESEM observation, all samples were gold coated. The nanofiber diameters were measured from the FESEM image using Digimizer4 software.

Results and Discussion

Effect of air resistance on jet trajectory

In centrifuge spinning, a strong airstream is produced by nozzle and nozzle receptacle. This airstream causes aerodynamic forces that deflect the jet and as a consequence, the liquid jet

progressively bends up. Therefore, nanofibers deposition would be influenced by airstream. Also, air resistance leads the enhancement of surface instabilities which cause to fabricate beaded nanofibers. In addition, exposing the ejected liquid jet to the high velocity airflow causes the jet to lose its solvent rapidly and as a consequence, the extension of the jet becomes more difficult, resulting in thicker nanofibers. It seems that if both the nozzle and the collector rotate at the same time and direction, air stream rotates as a rigid body. Therefore, the effects due to aerodynamic forces on the jet are negligible. However, preventing the air to exit and enter the spinning head confirms the isolation of spinning process.

To investigate the effect of air drag on jet trajectory, the fabrication process has been implemented using centrifuge spinning and air-sealed centrifuge spinning. Three fluids indicated in Table 1 have been used. Curved jets fabricated by centrifuge spinning and air-sealed centrifuge spinning are shown in figure2. It can be seen in figure 2 that non-isolated jets produced by centrifuge spinning are more deflected than isolated ones due to air drag. It can be concluded that air-sealed centrifuge spinning exclude from airstream. Therefore, surface instabilities due to air drag are decreased by air-sealed centrifuge spinning.

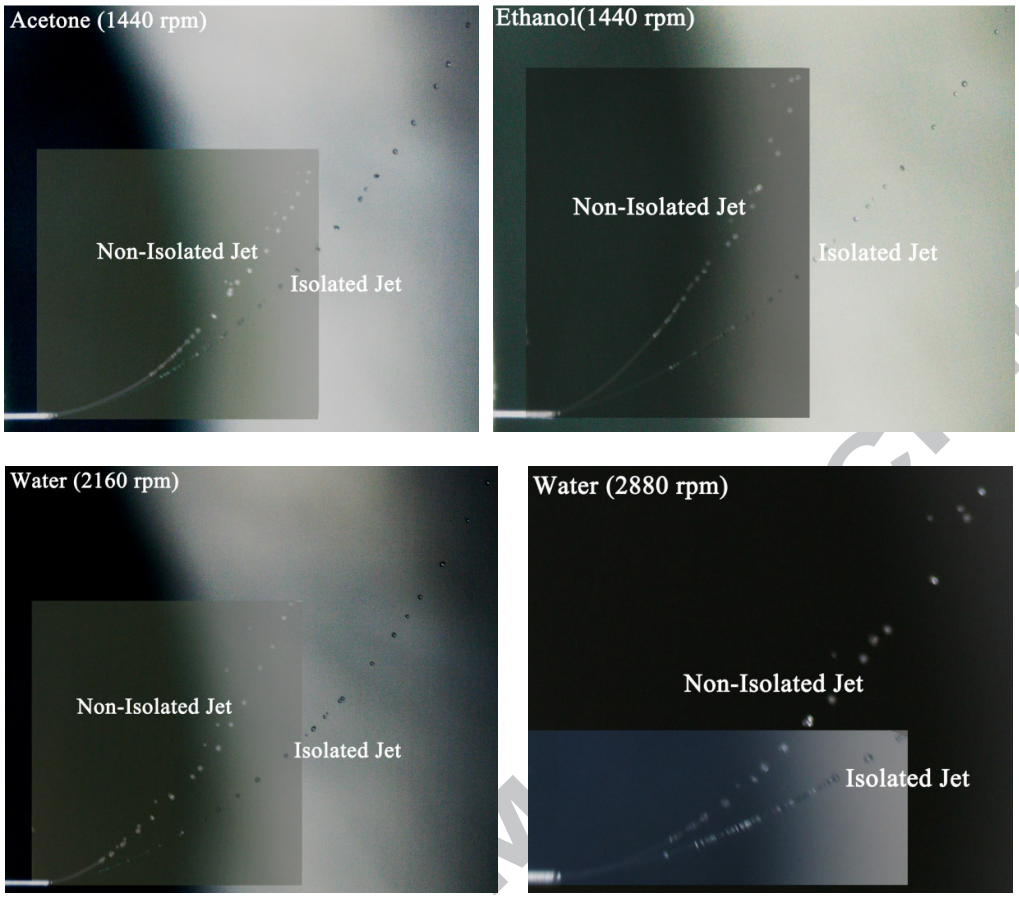

Figure 2, Jet trajectory for different liquids

Also, to indicate the real path of the polymeric jet in air-sealed centrifuge spinning, spinning process was carried out using a PAN/DMF solution and rotational speed of 2500 rpm. Figure 3(a) illustrates the real path of the jet in air-sealed centrifuge spinning system that was taken by high resolution Canon camera. Figure 3(a) shows that the jet travels in a straight trajectory instead of curved path and nanofiber mat is deposited in front of the nozzle. Also, no oscillation was observed in the centerline of the jet. Possible reason for these observations is neglibility of air resistance through air-sealed centrifuge spinning. The real path of the polymeric jet in centrifuge spinning is shown in figure 3(b). As shown in figure 3(b), the polymeric jet travels in a curved line. Also, the oscillations were observed in polymeric jet as shown in figure 3(b). As previously indicated centrifuge spinning was involved by a strong

airstream. One effect of air resistance in centrifuge spinning is the deflection of jet which tends to curve the jet.

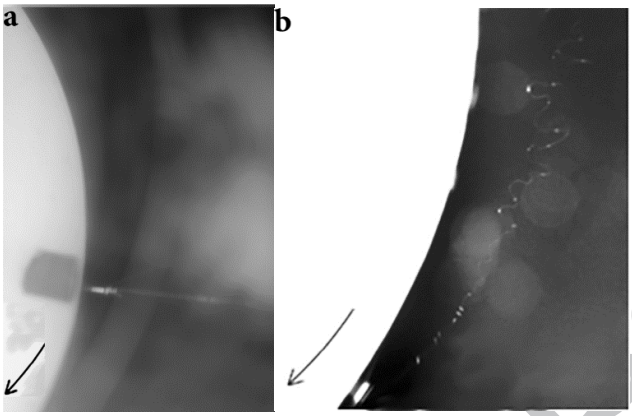

Figure 3. Polymer jet trajectory in (a) air-sealed centrifuge spinning [40] (b) centrifuge spinning [53]

Numerical Simulations of the Jet

A jet leaving a rotating orifice of radius *a* situated on the curved face of a cylindrical drum of radius s_0, which is rotating on its axis at a constant rate Ω was considered for simulation of fabrication process through air-sealed centrifuge spinning. The coordinate system used is an extension to cylindrical polar coordinates, (s, n, φ), where s is the arc-length along the jet and (n, φ) is polar coordinate in any cross section of the jet. This system was established and shown in more detail by Wallwark et al.[41]. The centerline was described by a Cartesian coordinate system (X(s, t), 0, Z(s, t)) in [41, 42]. We neglected the effects of the gravitational body force (setting g = 0). Also, the effects due to aerodynamic forces on the jet are negligible in the air-sealed centrifuge spinning due to its isolation. The forces including centrifugal (F_c), Coriolis (F_C), and viscous (F_{visc}) are experienced by the jet in air-sealed centrifuge spinning (figure 4).

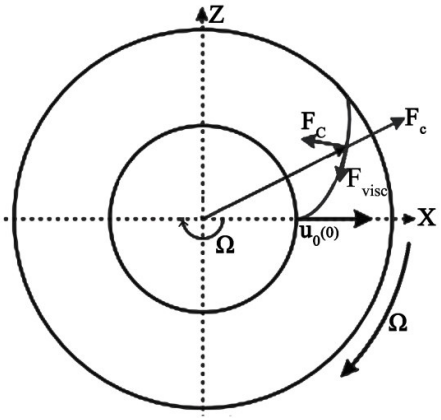

Figure 4, A schematic picture of the air-sealed centrifuge spinning

These assumptions provide the following Navier-Stokes equations of motion for a curved liquid jet in the inviscid and viscous cases, namely

$$\nabla . \vec{u} = 0 \qquad (1)$$

and

$$\frac{\partial \vec{u}}{\partial t} + (\vec{u} \,.\, \nabla)\, \vec{u} = -\frac{1}{\rho}\nabla p + \frac{\mu}{\rho}\nabla^2 \vec{u} - 2\,\vec{\Omega} \times \vec{u} - \vec{\Omega} \times (\vec{\Omega} \times \vec{r}) \qquad (2)$$

Where u, p, μ, and ρ are the velocity, the pressure, the viscosity, and the density of the jet; Ω is the angular velocity of the spinning head, r is the position vector in the rotating frame, , and t is the time. The free surface of the jet is given by $n = R(s, \varphi, t)$, where R is the radius of the jet. The conditions on the free surface are given by the kinematic condition, the tangential stress condition and the normal stress condition. The kinematic condition states that particles on the surface must remain on the surface,

$$\frac{D}{Dt}(R(s,\varphi,t) - n) = 0 \qquad (3)$$

The tangential stress condition and the normal stress condition are given by

$$[\![\boldsymbol{n}.\boldsymbol{\sigma}]\!].\mathbf{n} = \gamma k \quad (4)$$

$$[\![\boldsymbol{n}.\boldsymbol{\sigma}]\!].\mathbf{t} = 0 \quad (5)$$

Where **n** is the unit normal pointing away from the surface of the jet, **t** is the tangent vector, **σ** is the stress tensor and γ is the surface tension. *k* is the mean curvature of the free-surface.

The equations obtained from writing (1)–(5) in curvilinear coordinate are lengthy so they are not presented here but can be found in Paˇraˇu et al.[49]. A non-linear analysis of equations (1)–(5) was carried out by Paˇraˇu et al.[49].

The governing equations have been converted to dimensionless form using the following characteristic scales and dimensionless groups (overbars have been dropped, in final dimensionless equaions):

Characteristic Scales

Tangential velocity: $\bar{u} = \frac{u}{U}$

Radial velocity: $\bar{v} = \frac{v}{U}$

Azimuthal velocity: $\bar{\omega} = \frac{\omega}{U}$

Pressure: $\bar{p} = \frac{p}{\rho U^2}$

Radial point between the center and surface of the jet: $\bar{n} = \frac{n}{a}$

Radius of the jet: $\bar{R} = \frac{R}{a}$

Time: $\bar{t} = \frac{tU}{s_0}$

Arc-length coordinates: $\bar{X} = \frac{X}{s_0}$ and $\bar{Z} = \frac{Z}{s_0}$

Aspect ratio: $\epsilon = \frac{a}{s_0}$

Jet exit velocity: U

Dimensionless Groups

Reynolds number: $Re = \frac{\rho U a}{\mu}$

Rossby number: $Rb = \frac{U}{s_0 \Omega}$

Weber number: $We = \frac{\rho U^2 a}{\gamma}$

One-dimensional model equations were derived from the assumption that the flow is uniaxial and the center-line of the jet is steady at the leading order and it does not depend on time. The equations in the bulk are

$$(X_s Z_{ss} - X_{ss} Z_s)(u_0^2 - \frac{3}{Re} u_{0s} - \frac{1}{We R_0}) - \frac{2}{Rb} u_0 + \frac{(X+1)Z_s - Z X_s}{Rb^2} = 0 \quad (6)$$

$$u_0 u_{0s} = -\frac{1}{We}(\frac{1}{R_0})_s + \frac{Z Z + (X+1)X_s}{Rb^2} + \frac{3(R_0^2 u_{0s})_s}{Re R_0^2} \quad (7)$$

$$\frac{u_{0s}}{2} R_0 + u_0 R_{0s} = 0 \quad (8)$$

$$X_s^2 + Z_s^2 = 1 \quad (9)$$

It can be observed from Eq. 19 that $R_0^2 u_0$ is constant and, by using $R_0(0) = 1$ and $u_0(0) = 1$, we have $R_0^2 u_0 = 1$, therefore R_0 can be replaced by $1/\sqrt{u_0}$,

$$(X_s Z_{ss} - X_{ss} Z_s)(u_0^2 - \frac{3}{Re} u_{0s} - \frac{\sqrt{u_0}}{We}) - \frac{2}{Rb} u_0 + \frac{(X+1)Z_s - ZX_s}{Rb^2} = 0 \quad (10)$$

$$u_0 u_{0s} = -\frac{1}{We} \frac{u_{0s}}{2\sqrt{u_0}} + \frac{ZZ + (X+1)X_s}{Rb^2} + \frac{3}{Re}(u_{0ss} - \frac{u_{0s}^2}{u_0}) \quad (11)$$

$$X_s^2 + Z_s^2 = 1 \quad (12)$$

In order to solve the problem, a good initial guess must be provided for each solution step. The first initial guess required to get started was taken as a straight cylinder of constant radius, without rotation. The nonlinear equations are solved at each step using Newton's method. The previously calculated solution was used to provide initial guess for the next step.

Simulation and comparison with experiment

Jet trajectory: Newtonian fluids

The fluid material properties (Table 1) combined with the processing conditions indicated at Table 2, are used to obtain the dimensionless groups required in the simulation model.

The dimensionless parameter values (Table 2) are used in the simulation code, which allows the determination of a simulated jet trajectory. Experimental trajectory profiles for isolated and non-isolated jet are extracted from the experimental images as seen in figure 2. The experimental and simulated curves can now be directly compared.

Table 2. Processing parameters and dimensionless parameters of Newtonian fluids

Newtonian fluid	Processing parameters		Dimensionless parameters		
	Rotational speed (rpm)	Flow rate (ml/h)	Re	Rb	We
Water	1440	79.5	88	0.146	1.33
	2160	157	173.6	0.192	5.17

	2880	263	290.4	0.243	14.4
Ethanol	1440	72	52.32	0.132	2.8
Acetone	1440	144	349.3	0.265	11

It can be seen from figure 5 that the trajectory profile of the isolated water jet and simulation are in good agreement: the model is correctly predicting the trajectory of isolated water jet. Increasing the rotational speed causes more deflection of non-isolated jet. It can be deduced that the isolated jet has not experienced air drag, unlike non-isolated jet. There is a difference between trajectory of non-isolated water jet and simulation; particularly at higher speed. It is caused by increasing air drag with increasing rotational speed.

There is a little deflection between isolated acetone as well as ethanol jet and simulation (figure 6). However, there was still fairly good agreement between them. Also, the non-isolated jet of acetone as well as ethanol is more deflected than the simulation due to air drag.

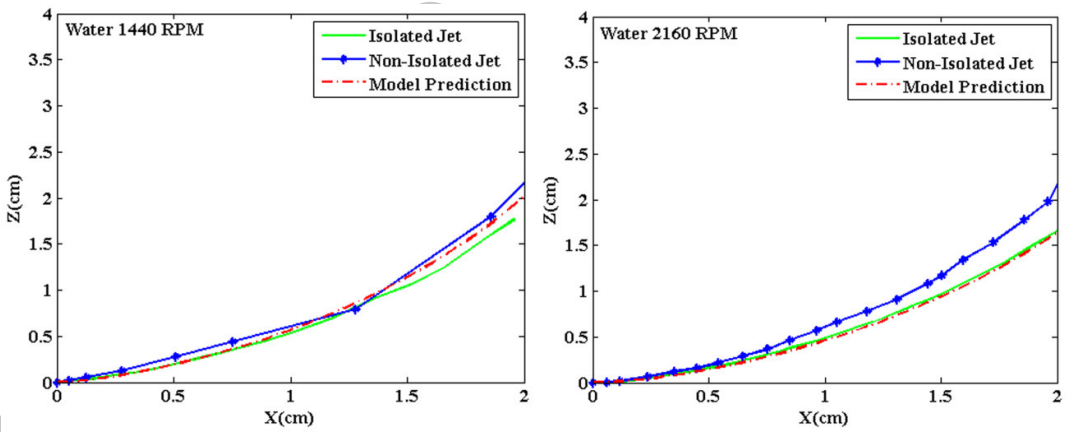

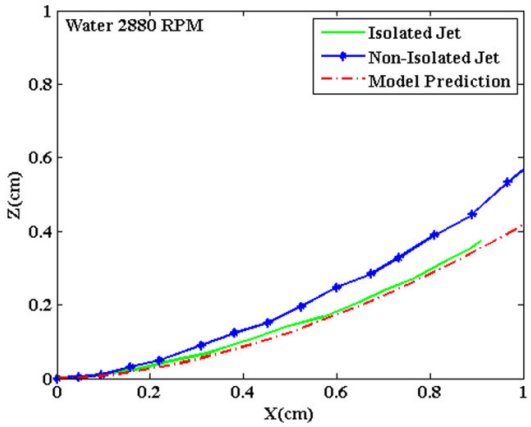

Figure 5, Jet trajectory for water: Isolated jet, Non-isolated jet, and Predicted Jet

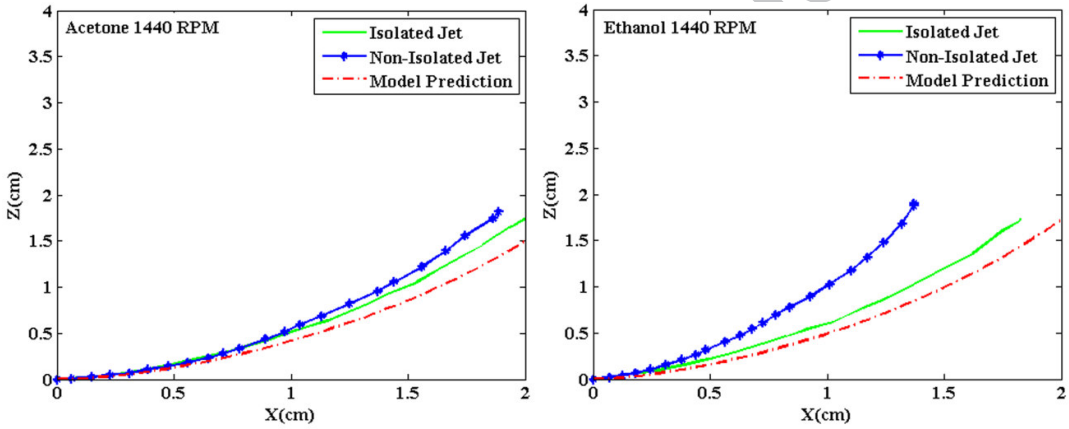

Figure 6, Jet trajectory for acetone and ethanol: Isolated jet, Non-isolated jet, and Predicted Jet

Jet radius: viscous fluid

As discussed in the introduction, the PAN solution as a viscous fluid has been spun through air-sealed centrifuge spinning. The fluid was spun under conditions indicated at Table 3. FESEM images of nanofibers fabricated by air-sealed centrifuge spinning at different rotational speeds are shown in figure 7. Previously, Valipouri et.al. [40] found that nanofibers manufactured by centrifuge spinning are much thicker than those produced by air-sealed

centrifuge spinning. In fact, the jet in centrifuge spinning is exposed to the strong airstream, which increases the evaporation rate of jet solvent. Therefore, the elongational viscosity of the jet reaches to a level that makes any further deformation (stretching) impossible [40].

Table 3. Processing parameters for spinning of PAN solution and dimensionless parameters

Processing parameters		Dimensionless parameters		
Rotational speed (rpm)	Flow rate (ml/h)	Re	Rb	We
2160	0.2862	4.08×10^{-4}	3.53×10^{-4}	3.33×10^{-5}
2880	0.5724	8.16×10^{-4}	5.315×10^{-4}	1.33×10^{-4}
3600	0.7111	1.02×10^{-3}	5.31×10^{-4}	2.08×10^{-4}
4320	0.9598	1.36×10^{-3}	5.88×10^{-4}	3.68×10^{-4}

Mean diameter of all samples is indicated at Table 4. It can be seen from the FESEM images that increasing the rotational speed of spinning head tends to increase nanofiber diameter. Diameter of nanofibers fabricated at 2160 rpm is 171 nm, while nanofibers diameter at rotational speed of 2880, 3600, and 4320 rpm, was determined as 216, 212, and 220 nm respectively. Centrifugal force as an extensional force causes to the jet to be extended. Therefore, it is expected to fabricate finer fibers with increasing rotational speed, whereas nanofiber diameter increased by increasing rotational speed, here. Increasing rotational speed from 2160 rpm to 4320 rpm causes to highly increase flow rate from 0.2862 to 0.9598 ml/h. It was found that lower flow rates yielded fibers with smaller diameters [54]. Too high flow rates resulted in thicker fibers, as they do not get enough time to dry before reaching the collector[55, 56].

Table 4. PAN nanofiber diameter: experimental and simulation

Rotational speed	Experimental nanofiber	Simulation predicted jet diameter
2160	171	0.0139
2880	216	0.0163
3600	212	0.0160
4320	220	0.0167

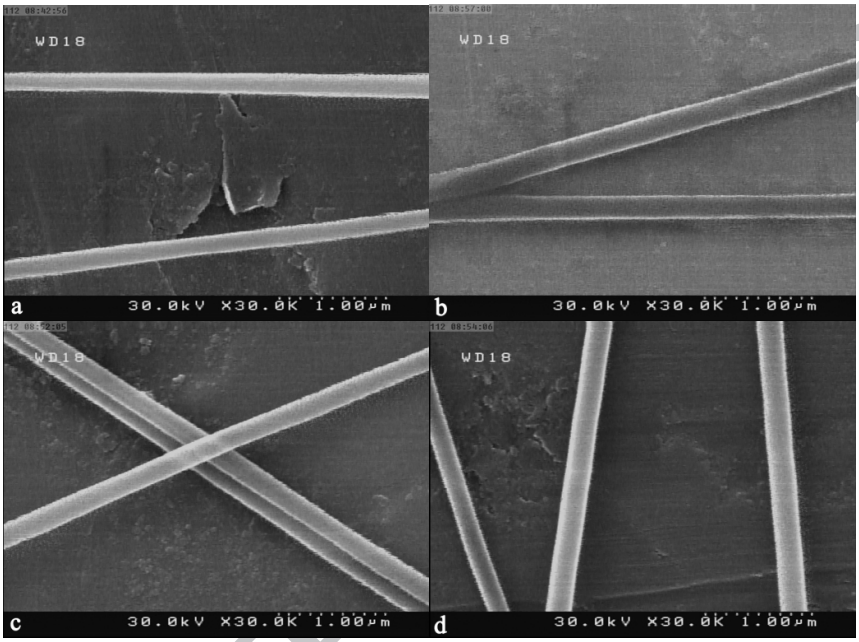

Figure 7, FESEM images of PAN nanofibers fabricated via air-sealed centrifuge spinning at rotational speed of: (a) 2160 rpm (b) 2880 rpm (c) 3600 rpm (d) 4320 rpm

Using the spinning conditions indicated at Table 3, the dimensionless groups for quantitative simulation can be determined. These values of the dimensionless groups (Table 3) are used to simulate expected jet radius profiles as well as jet trajectory through air-sealed centrifuge spinning. The predicted jet radius profiles can then be compared with experiment. It can be seen from figure 8 that with increasing the rotational speed, the jet path expands farther from the nozzle. However, all jets have the same trajectory during the first step near the nozzle. The jet diameter as a function of arc length was plotted and is shown in figure 9. There is a

little difference between all trends. It can be seen from the asymptote of all curves that the jet diameter at 2160 rpm is less than others. The simulated diameters of all samples are 0.0139, 0.0163, 0.0160, and 0.0167 DU at 2160, 2880, 3600, and 4320 rpm respectively in dimensionless arc length, 2.4 units (Table 4). This prediction precisely matches the trend observed for the influence of rotational speed in the experiments. Also, like the experimental result the jet diameter at rotational speed of 2880, 3600, and 4320 are approximately similar to each other.

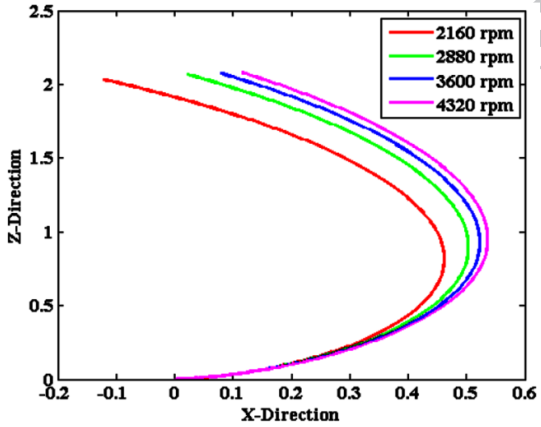

Figure 8, Predicted steady trajectory for PAN solution jet at different rotational speed

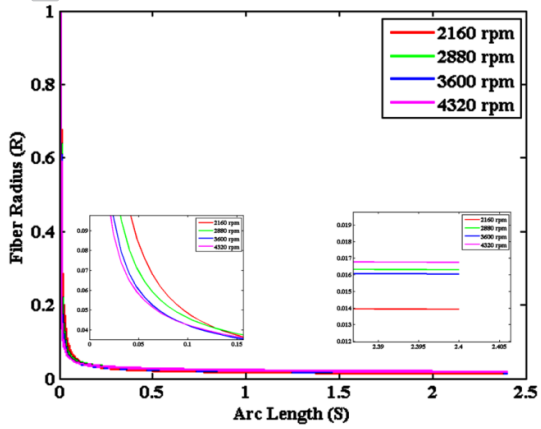

Figure 9, Predicted PAN jet radius vs arc length at different rotational speed

Conclusion

We have demonstrated that air-sealed centrifuge spinning is released from airstream and air drag. A comparison between an isolated and a non-isolated curved jet emerging from a rotating nozzle has been carried out through air-sealed centrifuge spinning as well as centrifuge spinning system. Images were captured of the jet trajectory using a high speed camera. Non-isolated jets were more curved than isolated jets due to air resistance. The experimental results were compared to numerical solutions to the Navier–Stokes equations. There was fairly good agreement between isolated jet trajectory and model-predicted one, but there were differences between non-isolated jet trajectory and simulation results. The non-isolated jet curved more compared to others duo to air drag. Also, the diameter of PAN nanofibers was predicted and compared with experiments. There is the same trend in nanofiber diameter with increasing rotational speed in both experiment and simulation.

References:

[1] W. A. G. III, D. Brenner, S. E. Lyshevski, and G. J. Iafrate, Eds., *Handbook of Nanoscience, Engineering, and Technology*. CRC Press, 2007, p.^pp. Pages.

[2] V. EA, d. V. B. NC, d. B. J, and d. Q. AA, Hyperbranched polyglycerol electrospun nanofibers for wound dressing applications, Acta Biomaterialia, Vol. 6, pp. 1069-1078, 2010.

[3] Z. Xie, C. B. Paras, H. Weng, P. Punnakitikashem, L.-C. Su, K. Vu, *et al.*, Dual growth factor releasing multi-functional nanofibers for wound healing Acta Biomaterialia, Vol. In Press, p. Available online, 2013.

[4] M. A. Hassan, B. Y. Yeom, A. Wilkie, B. Pourdeyhimi, and S. A. Khan, Fabrication of nanofiber meltblown membranes and their filtration properties, Journal of Membrane Science, Vol. 427, pp. 336-344, 2013.

[5] D. Cho, A. Naydich, M. W. Frey, and Y. L. Joo, Further improvement of air filtration efficiency of cellulose filters coated with nanofibers via inclusion of electrostatically active nanoparticles, Polymer, Vol. 54, pp. 2364-2372, 2013.

[6] W. W.-F. Leung, C.-H. Hung, and P.-T. Yuen, Effect of face velocity, nanofiber packing density and thickness on filtration performance of filters with nanofibers coated on a substrate Separation and Purification Technology

Vol. 71, pp. 30-37, 2010.

[7] P. W. Gibson, C. Lee, F. Ko, and D. Reneker, Application of Nanofiber Technology to Nonwoven Thermal Insulation Journal of Engineered Fibers and Fabrics Vol. 2 pp. 32-40, 2007.

[8] Z. Rui, J. Chang-Yun, L. Xi-Zhe, L. Bin, K. Abhishek, and S. Ramakrishna, Improved adhesion of interconnected TiO2 nanofiber network on conductive substrate and its application in polymer photovoltaic devices, Applied Physics Letters, Vol. 93, pp. 013102-013102-3, 2008.

[9] M. M. Bergshoef and G. J. Vancso, Transparent nanocomposites with ultrathin electrospun nylon-4,6 fiber reinforcement, Advanced Materials, Vol. 11, pp. 1362–1365, 1999.

[10] T. Ondarcuhu and C. Joachim, Drawing a single nanofibre over hundreds of microns, Europhysics Letters, Vol. 42, pp. 215–220, 1998.

[11] L. Feng, S. Li, H. Li, J. Zhai, Y. Song, L. Jiang, *et al.*, Super-Hydrophobic Surface of Aligned Polyacrylonitrile Nanofibers, Angewandte Chemie International Edition, Vol. 41, pp. 1221-1223, 2002.

[12] C. R. Martin, Membrane-based synthesis of nanomaterials, Chemistry of Materials Vol. 8, pp. 1739–1746, 1996.

[13] G. J. Liu, J. F. Ding, L. J. Qiao, A. Guo, B. P. Dymov, J. T. Gleeson, *et al.*, Polystyrene-block-poly (2-cinnamoylethyl methacrylate) nanofibers-Preparation, characterization, and liquid crystalline properties, Chem-A European J, Vol. 5, pp. 2740–2749, 1999.

[14] Z. M. Huang, Y. Z. Zhang, M. Kotaki, and S. Ramakrishna, A review on polymer nanofibers by electrospinning and their applications in nanocomposites, Composites Science and Technology, Vol. 63, pp. 2223–2253, 2003.

[15] D. Li and Y. N. Xia, Electrospinning of nanofibers: Reinventing the wheel? , Advanced Materials, Vol. 16, pp. 1151-1170, 2004.

[16] S. V. Fridrikh, J. H. Yu, M. P. Brenner, and G. C. Rutledge, Controlling the Fiber Diameter during Electrospinning, Physical Review Letters, Vol. 90, p. 144502, 2003.

[17] Y. Yamashita, F. Ko, A. Tanaka, and H. Miyake, Characteristics of Elastomeric Nanofiber Membranes Produced by Electrospinning, Journal of Textile Engineering Vol. 53, pp. 137-142, 2007.

[18] S. Paruchuri and M. P. Brenner, Splitting of a liquid jet, physical review letters, Vol. 98, p. 134502, 2007.

[19] G. H. Kim, Y.-S. Cho, and W. D. Kim, Stability analysis for multi-jets electrospinning process modified with a cylindrical electrode European Polymer Journal, Vol. 42, pp. 2031-2038, 2006.

[20] Y. Srivastava, M. Marquez, and T. Thorsen, Multijet electrospinning of conducting nanofibers from microfluidic manifolds, Journal of Applied Polymer Science, Vol. 106, pp. 3171–3178, 2007.

[21] S. A. Theron, A. L. Yarin, E. Zussman, and E. Kroll, Multiple jets in electrospinning: experiment and modeling, Polymer, Vol. 46, pp. 2889-2899, 2005.

[22] W. Tomaszewski and M. Szadkowski, Investigation of Electrospinning with the Use of a Multi-jet Electrospinning Head, FIBRES & TEXTILES in Eastern Europe Vol. 13, pp. 22-26, 2005.

[23] A. Vaseashta, Controlled formation of multiple Taylor cones in electrospinning process Applied Physics Letters, Vol. 90, p. 093115, 2007.

[24] A. Varesano, F. Rombaldoni, G. Mazzuchetti, C. Tonin, and R. Comotto, Multi-jet nozzle electrospinning on textile substrates: observations on process and nanofibre mat deposition, Polym Int, Vol. 59, pp. 1606–1615, 2010.

[25] S. Xie and Y. Zeng, Effects of Electric Field on Multineedle Electrospinning: Experiment and Simulation Study, Ind. Eng. Chem. Res., Vol. 51, p. 5336 – 5345, 2012.

[26] A. Varesano, R. A. Carletto, and G. Mazzuchetti, Experimental investigations on the multi-jet electrospinning process, Journal of Materials Processing Technology Vol. 209, pp. 5178–5185, 2009.

[27] Y. Yamashita, F. Ko F, H. Miyake, and A. Higashiyama, Establishment of nanofiber preparation technique by electrospinning, Sen'i Gakkaishi, Vol. 64, pp. 24–28, 2008.

[28] A. L. Yarin and E. Zussman, Upward needleless electrospinning of multiple nanofibers, Polymer, Vol. 45, pp. 2977-2980, 2004.

[29] Y. Liu and J.-H. He, Bubble Electrospinning for Mass Production of Nanofibers, International Journal of Nonlinear Sciences and Numerical Simulation, Vol. 8, pp. 393-396, 2007.

[30] O. O. Dosunmu, G. G. Chase, W. Kataphinan, and D. H. Reneker, Electrospinning of polymer nanofibres from multiple jets on a porous tubular surface, Nanotechnology, Vol. 17, pp. 1123–1127, 2006.

[31] O. Jirsak, P. Sysel, F. Sanetrnik, J. Hruza, and J. Chaloupek, Polyamic Acid Nanofibers Produced by Needleless Electrospinning, Journal of Nanomaterials, Vol. 2010, p. Article ID 842831, 2010.

[32] X. Wang, H. Niu, X. Wang, and T. Lin, Needleless Electrospinning of Uniform Nanofibers Using Spiral Coil Spinnerets, Journal of Nanomaterials, Vol. 2012 p. Article ID 785920, 2012

[33] F. L. Zhou, R. H. Gong, and I. Porat, Polymeric Nanofibers via Flat Spinneret Electrospinning, Polym. Eng. Sci. , Vol. 49, pp. 2475–2481, 2009.

[34] J. S. Varabhas, G. G. Chase, and D. H. Reneker, Electrospun nanofibers from a porous hollow tube, Polymer Vol. 49, pp. 4226–4229, 2008.

[35] A. Kumar, M. Wei, C. Barry, J. Chen, and J. Mead, Controlling Fiber Repulsion in Multijet Electrospinning for Higher Throughput, Macromol. Mater. Eng., Vol. 295, pp. 701–708, 2010.

[36] K. Sarkar, C. Gomez, S. Zambrano, M. Ramirez, E. d. Hoyos, H. Vasquez, *et al.*, Electrospinning to forcespinning™, Materials Today, Vol. 13, pp. 12-14, 2010.

[37] M. R. Badrossamay, H. A. McIlwee, J. A. Goss, and K. K. Parker, Nanofiber Assembly by Rotary Jet-Spinning, Nano Letters Vol. 10, pp. 2257–2261, 2010.

[38] S. Padron, A. Fuentes, D. Caruntu, and K. Lozano, Experimental study of nanofiber production through forcespinning, JOURNAL OF APPLIED PHYSICS Vol. 113, pp. 024318-9, 2013.

[39] A. Bellofiore, EXPERIMENTAL AND NUMERICAL STUDY OF LIQUID JETS INJECTED IN HIGH-DENSITY AIR CROSSFLOW Ph.D., DEPARTMENT OF CHEMICAL ENGINEERING UNIVERSITY OF STUDIES OF NAPLES FEDERICO II 2005-2006

[40] A. Valipouri, S. A. H. Ravandi, and A. Pishevar, A novel method for manufacturing nanofibers, Fibers and Polymers, Vol. 14, pp. 941-949, 2013.

[41] I. M. WALLWORK, S. P. DECENT, A. C. KING, and R. M. S. M. SCHULKES, The trajectory and stability of a spiralling liquid jet. Part 1. Inviscid theory, Journal of Fluid Mechanics Vol. 459, pp. 43-65, 2002.

[42] S.P. DECENT, A.C. KING, and I. M. WALLWORK, Free jets spun from a prilling tower, Journal of Engineering Mathematics, Vol. 42, pp. 265-282, 2002.

[43] S. P. Decent, A. C. King, M. J. H. Simmons, E. I. Paˇraˇu, I. M. Wallwork, C. J. Gurney, *et al.*, The trajectory and stability of a spiralling liquid jet: Viscous theory, Applied Mathematical Modelling, Vol. 33, pp. 4283–4302, 2009.

[44] J.-M. Vanden-Broeck and J. B. Keller, Jets rising and falling under gravity, Journal of Fluid Mechanics, Vol. 124, pp. 335–345, 1982.

[45] M. V. Entov and A. L. Yarin, The dynamics of thin liquid jets in air, Journal of Fluid Mechanics, Vol. 140, pp. 91–111, 1984.

[46] F. Dias and J.-M. Vanden-Broeck, Flows emerging from a nozzle and falling under gravity, Journal of Fluid Mechanics, Vol. 213, pp. 465–477, 1990.

[47] A. Yarin, *Free Liquid Jets and Films: Hydrodynamics and Rheology*: Longman, New York 1993.

[48] L. J. Cummings and P. D. Howell, On the evolution of non-axisymmetric viscous fibres with surface tension, inertia and gravity, Journal of Fluid Mechanics, Vol. 389, pp. 361–389, 1999.

[49] E. I. P˘ar˘au, S. P. Decent , M. J. H. Simmons, D. C. Y. Wong, and A. C. King, Nonlinear viscous liquid jets from a rotating orifice, J Eng Math, Vol. 57, 2007.

[50] C. P. Carroll and Y. L. Joo, Electrospinning of viscoelastic Boger fluids: Modeling and experiments, Physics of Fluids, Vol. 18, pp. 053102-14, 2006.

[51] J. J. Feng, The stretching of an electrified non-Newtonian jet: A model for electrospinning, Physics of Fluids, Vol. 14, pp. 3912-3926, 2002.

[52] D. H. Reneker, A. L. Yarin, H. Fong, and S. Koombhongse, Bending instability of electrically charged liquid jets of polymer solutions in electrospinning, Journal of Applied Physics, Vol. 87, pp. 4531-4547, 2000.

[53] F. Dabirian, S. A. H. Ravandi, and A. R. Pishevar, Investigation of Parameters Affecting PAN Nanofiber Production Using Electrical and Centrifugal Forces as a Novel Method Current Nanoscience, Vol. 6, pp. 545-552, 2010.

[54] X. Zong, K. Kim, D. Fang, S. Ran, B.S. Hsiao, and B. Chu, Structure and process relationship of electrospun bioabsorbable nanofiber membranes, Polymer, Vol. 43, pp. 4403–4412, 2002.

[55] W. Zuo, M. Zhu, W. Yang, H. Yu, Y. Chen, and Y. Zhang, Experimental Study on Relationship Between Jet Instability and Formation of Beaded Fibers During Electrospinning, Polymer Engineering and Science, pp. 704-709, 2005.

[56] C. X. Zhang, X. Y. Yuan, L. L. Wu, Y. Han, and J. Sheng, Study on morphology of electrospun poly(vinyl alcohol) mats, European Polymer Journal, Vol. 41 pp. 423-432, 2005.

- We present a novel method for the fabrication of ultrafine polymeric nanofibers.
- Air-sealed centrifuge spinning was skillfully sealed from ambient airflow.
- The liquid jet trajectory in centrifuge spinning and novel method was compared.
- Non-isolated jets were more curved than isolated ones due to air resistance.
- There was a good agreement between isolated jet trajectory and model-predicted one.